26. D. L. Caspar, *Biophys. J.* **32**, 103 (1980).
27. For additional data, see *Science* Online (www.sciencemag.org/feature/data/1052183.shl).
28. Based on a comparison of light-scattering intensities for His_{10}-tagged NM in the presence of 50 μM $ZnCl_2$, which converts most of the protein to oligomeric species (*17*).
29. Fibers were stable to 8 M urea and 2% SDS, whereas the monomer:oligomer equilibrium was altered even by changes in temperature and salt concentration.
30. By TEM, even the overnight rotation (60 rpm) did not fracture mature fibers. In addition, rotated fibers seeded the fibrillization of fresh NM at a rate similar to that of seeding by unagitated fibers (*17*).
31. The slow phase in preincubated reactions may represent either the addition of monomers or the rate at which the intermediate is formed.
32. J. R. Glover and S. Lindquist, *Cell* **94**, 73 (1998).
33. E. U. Weber-Ban, B. G. Reid, A. D. Miranker, A. L. Horwich, *Nature* **401**, 90 (1999).
34. S. Lindquist and E. C. Schirmer, in *Molecular Chaperones and Folding Catalysts. Regulation, Cellular Function and Mechanisms*, B. Bukau, Ed. (Harwood, Amsterdam, 1999), pp. 347–380.
35. T. R. Serio and S. L. Lindquist, *Annu. Rev. Cell Dev. Biol.* **15**, 661 (1999).
36. Our data, therefore, indicate that the effects of Sup35 concentrations on [PSI^+] induction in vivo reflect alterations in the ratio of the prion protein to Hsp104 and other cellular factors, rather than in the intrinsic folding and conversion properties of Sup35.
37. K. A. Dill, *Protein Sci.* **8**, 1166 (1999).
38. P. T. Lansbury Jr., *Proc. Natl. Acad. Sci. U.S.A.* **96**, 3342 (1999).
39. K. H. Mayo, *Trends Biotechnol.* **18**, 212 (2000).
40. T. R. Serio, A. G. Cashikar, J. J. Moslehi, A. S. Kowal, S. L. Lindquist, *Methods Enzymol.* **309**, 649 (1999).
41. Because of sensitivity limitations in CR binding at low protein concentration and CD at high protein concentrations, both methods were used across the broad concentration range tested. Further, stirred reactions for CD proceeded faster than unstirred reactions for CR binding.
42. J. S. Wall and J. F. Hainfeld, *Annu. Rev. Biophys. Biophys. Chem.* **15**, 355 (1986).
43. We thank T. Scheibel for plasmid pJC25NMstop (6798) and advice; M. Simon, B. Lin, J. Wall, and the Brookhaven National Laboratory for assistance with STEM; members of the Lindquist lab for comments and discussion; S. Xu and B. Bevis for assistance with AFM; and the National Institutes of Health (GM025874, P41-RR017777, GM57840), the Howard Hughes Medical Institute, U.S. Department of Energy, Office of Biological and Environmental Research, the Keck Foundation (991705), Materials Research Science and Engineering Centers (DMR 9808595), and the Cancer Fund of the Damon Runyon–Walter Winchell Foundation (DRG-1436) for financial support.

15 May 2000; accepted 3 July 2000

Hydrological Impact of Heinrich Events in the Subtropical Northeast Atlantic

Edouard Bard,[1]* Frauke Rostek,[1] Jean-Louis Turon,[2] Sandra Gendreau[2]

Reconstructing the impact of Heinrich events outside the main belt of ice rafting is crucial to understanding the underlying causes of these abrupt climatic events. A high-resolution study of a marine sediment core from the Iberian margin demonstrates that this midlatitude area was strongly affected both by cooling and advection of low-salinity arctic water masses during the last three Heinrich events. These paleoclimatic time series reveal the internal complexity of each of the last three Heinrich events and illustrate the value of parallel studies of the organic and inorganic fractions of the sediments.

High-resolution paleoclimatic records show that the glacial climate was far more variable than previously thought. Studies of North Atlantic sediments show that the circulation of the surface and deep waters was repeatedly perturbed by massive surges and melting of icebergs. Although most researchers would agree that these so-called Heinrich (H) events originated from the Laurentide ice sheets (*1–6*), there is growing controversy about the precise behavior of other ice sheets during these events [see recent works on lithological indices (*7, 8*) and studies based on the Sr-Nd isotopic signatures of ice-rafted detritus (IRD) (*9, 10*)].

The influence of Heinrich events has sometimes been invoked to explain unusual high-frequency climatic events at low latitudes [e.g., (*11*)]. Abrupt decreases of sea surface temperature (SST) in phase with Heinrich events were detected in sediments of the Bermuda Rise (*12*) and the Mediterranean Sea (*13*). Further south, the tropical western Atlantic apparently warmed during H1 and the Younger Dryas (YD) (*14*). The strong, direct effect of melting icebergs is generally thought to be restricted to a North Atlantic belt between 40°N and 55°N, where IRD forms distinct layers in the sediments (*15*). The occurence and climatic impact of H events are still poorly documented in the northeast Atlantic, especially at subtropical latitudes.

To reveal the impact of H events on the northeast Atlantic, we focused our study on the paleoceanographic variability in a midlatitude core from the Iberian margin (SU8118 located at 37°46′N, 10°11′W and 3135 m depth) (Fig. 1). One of the main advantages of using SU8118 is that it is one of the best-dated cores available for the last deglaciation (*16*). These sediments are characterized by a high sedimentation rate (>20 cm/1000 years during the glacial and deglacial sections) which has been constrained by numerous ^{14}C accelerator mass spectrometry (AMS) ages and stable isotope records (*17*).

SST changes were reconstructed with the alkenone unsaturation ratios (Fig. 2B and Web table 1) (*18, 19*), and counts of IRD (Fig. 2B and Web table 1) (*18, 20*) and magnetic susceptibility (MS; Fig. 2B) (*21*) were used to identify transported sediments. The alkenone temperature estimates are on the order of 18°C during the last 5000 years, which is between the modern annual mean (17.5°C) and the SST during summer months (19°C) when most of the local primary productivity takes place. With an average sampling resolution of ~250 years, the alkenone-SST record shows the classical climate history of the Late Glacial: the Holocene starts at 11,500 calendar years before present (cal yr B.P.), the YD event is centered at about 12,000 cal yr B.P., and the Allerød-Bølling interstadial occurs between 13,000 and 15,000 cal yr B.P. Interestingly, the LGM in the strictest sense (21,000 ± 2000 cal yr B.P.) is a rather mild period, with SST on the order of 13°C, i.e., about 5°C lower than modern SST. In addition, the glacial period is characterized by a rather large variability with abrupt cold spells centered at about 16,000, 23,500, 26,000, and 31,000 cal yr B.P.

Figure 2B shows the IRD counts and the MS record which can be used to identify detrital material usually attributed to H events. These are clearly expressed in both records between 18,000 and 15,500 cal yr B.P. for H1 and between 26,000 and 23,000 cal yr B.P. for H2. The MS and mineralogical records (*20*) also suggest that each of these two events were complex and characterized by two depositional phases centered at 16,000 (H1a) and 17,500 (H1b) cal yr B.P. for H1 and at 23,500 (H2a) and 25,000 (H2b) cal yr B.P. for H2. Our results

[1]Centre Européen de Recherche et d'Enseignement en Géosciences de l'Environnement (CEREGE), UMR 6635, CNRS, and Université d'Aix-Marseille III, Europôle de l'Arbois, 13545 Aix-en-Provence cedex 4, France. [2]Département de Géologie et Océanographie (DGO), UMR EPOC 5805, CNRS and Université de Bordeaux I, Avenue des Facultés, 33405 Talence cedex, France.

*To whom correspondence should be addressed. E-mail: bard@cerege.fr

strengthen earlier suggestions of twinned IRD peaks in some cores of the Portuguese margin (*22*). Interestingly, only the late depositional phases are well expressed in the IRD records: there is a lack of IRD at about 25,000 cal yr B.P. and only a slight increase around 17,500 cal yr B.P. An alternative explanation of the multiple peaks is that they belong to the pervasive millennial-scale cycle that consistently punctuates the intervals between H events and the Holocene period (*2*). Furthermore, the alkenone-SST record is also characterized by small shifts at about 21,500 and 29,000 cal yr B.P. (Fig. 2A) which may be explained by the same cyclicity (the latter cooling is even associated with an MS peak).

H3 may be only partly expressed in core SU8118, because the oldest sediment in this core is about 31,500 cal yr B.P. However, it is clear that the SST decrease and MS increase measured in the lowermost section do indeed correspond to H3 even though there is no IRD increase in the same sediment levels. Low IRD concentrations during H3 have already been described in sediments of the main IRD belt (*3*), north of the Azores (*23*), and off Portugal (*24*) [although a small IRD peak was detected farther offshore (*22*)]. The sole presence of an MS signal could be accounted for if the material transported by icebergs was all finer than 150 μm.

From Fig. 2, A and B, it is clear that strong and sharp cooling events coincide with all phases of H events H1a and H1b, H2a and H2b, and H3. It is worth noting that Zhao *et al.* (*25*) observed alkenone-SST drops off Mauritania roughly synchronous with H events, although the tentative chronology of their cores was not directly based on ^{14}C data. Their claim of an impact of H events on the Canary current was rather unexpected at the time and has awaited further confirmation. Our well-dated alkenone-SST record now provides a further proof that all latitudes of the eastern North Atlantic were strongly affected by these cooling events. By contrast, the western part of the low-latitude Atlantic appears to have warmed during YD and H1, as reconstructed with alkenones (*14*). Collectively, the observations based on alkenones indicate a significant increase (+3°C) in the east-west gradient of SST of the low-latitude North Atlantic during these two recent climatic events.

A by-product of the alkenone analyses in SU8118 is the discovery of large and systematic variations of the abundance of tetra-unsaturated C_{37} alkenones ($C_{37:4}$, molecular mass of 526). Percentages higher than 5% of the total C_{37} alkenones are restricted to very distinct periods centered around 31,000, 23,500, and 16,000 cal yr B.P. (Fig. 2C). These distinct $C_{37:4}$ peaks are clearly synchronous with H3, H2a, H1a, and H1b. We also note an absence of such a peak during event H2b and a rather weak signal during the YD event.

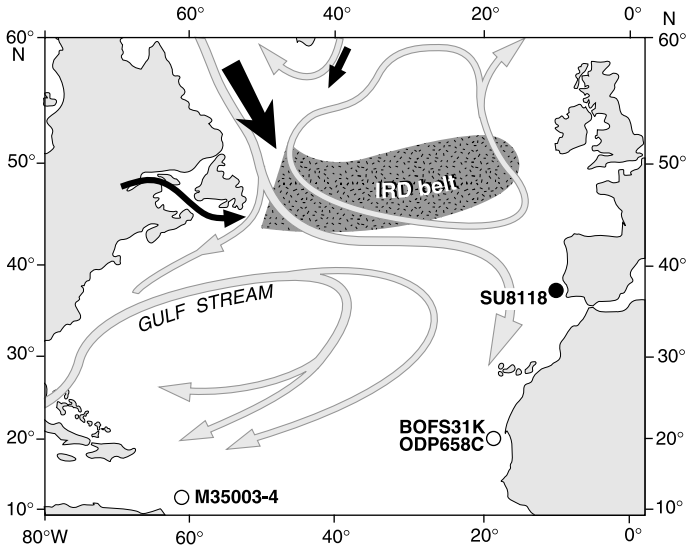

Fig. 1. Map showing North Atlantic cores located outside the main IRD belt and for which alkenone data are available to study the last 30,000 years. Black arrows indicate likely sources of icebergs, whereas the gray arrows represent the inferred circulation compiled by several authors (*32*).

Although the abundance of $C_{37:4}$ alkenone was originally used for paleothermometry (*26, 27*), Sikes *et al.* (*28*) analyzed coretops from the Southern ocean and suggested that this compound may not actually be linked to SST. Subsequently, Rosell-Melé (*29*) proposed that this particular alkenone is linked to low-salinity water masses and that a $C_{37:4}$ increase of about 5 to 10% corresponds to a freshening of one practical salinity unit (PSU). Further research is still needed to decipher if indeed salinity has a direct effect on the $C_{37:4}$ biosynthesis or if the observed pattern is due to a metabolic difference of coccolithophorids endemic of arctic or coastal water masses (*30*). Even if this latter hypothesis is confirmed, the $C_{37:4}$ abundances may still be used to study the surface advection of iceberg-bearing water masses together with their living arctic alkenone producers. In any case, $C_{37:4}$ levels in SU8118 are similar during the LGM and the Holocene, which indicates that this molecule is not simply correlated to SST because it behaves differently than the more abundant di- ($C_{37:2}$) and tri-unsaturated ($C_{37:3}$) methyl ketones used in the $U^{K'}_{37}$ index.

Applying the Rosell-Melé (*29*) calibration to our $C_{37:4}$ record leads to the conclusion that the salinity dropped by 1 to 2 PSU off Portugal during the last of the H events. This is in agreement with a salinity decrease of 2 to 3 PSU inferred for H1 which was based on $\delta^{18}O$ measurements in planktonic foraminifera from the same sediments (*31*). This salinity drop is comparable in magnitude to other salinity estimates inferred from cores located farther north in the Atlantic and thus closer to the former continental ice sheets (*29, 32*). Even if these salinity estimates remain semiquantitative, there is a rather impressive correlation between the $C_{37:4}$ fluctuations and the lithological variations used to identify H events (Fig. 2, B and C). Furthermore, the precise timing of these $C_{37:4}$ peaks is obviously not accidental and matches previous geochronological estimates for the abrupt H events (*3, 7*).

All available data from SU8118 suggest that advected high-latitude water transported icebergs that melted in the Iberian margin and released fine-grained detrital material. However, several differences are observed between the various proxies measured, particularly for events H2a (high MS but lack of IRD and $C_{37:4}$) and H3 (lack of IRD but high $C_{37:4}$ and MS). These peculiar signatures could be explained if icebergs did not transport the same amount of IRD during all phases of H events. This may indicate that there were multiple origins of ice during the surge events, such as from different parts of the Laurentide Ice Sheet or even from other sources such as the Fennoscandian Ice Sheet. The observed complexity may also be related to the size fraction of IRD: in distal layers, remote from all glacial sources, part of the mineralogical signal is carried by relatively fine detrital particles which would be expressed in the MS but not in the IRD counts (>150 μm).

Several authors recognized that H3 presents some unusual features compared to other H events (*1–4, 33*). Gwiazda *et al.* (*33*) even proposed that, when it is present, the IRD concentration peak could be due to a lack of foraminifera caused either by dissolution or low primary productivity, and they concluded that the iceberg discharge melted mostly in the western basin of the North Atlantic. The absence in core SU8118 of an IRD peak during H3 would be compatible with this theory, but the $C_{37:4}$, SST, and MS records strongly suggest that meltwater reached the eastern basin of the North Atlantic during this period. Independent evaluation of salinity changes may also be possible from the simultaneous analyses of Mg/Ca and $\delta^{18}O$ in the same shells of planktonic foraminifera (*34*).

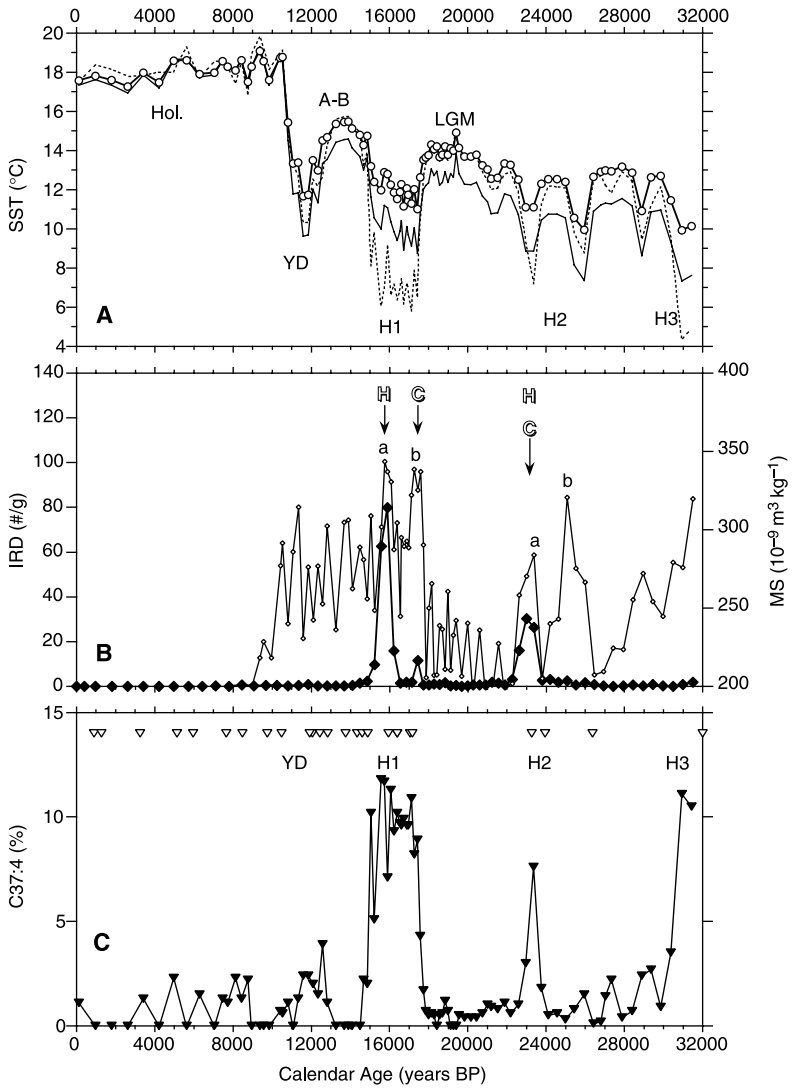

Fig. 2. New paleoclimatic records measured in core SU8118 represented versus calendar age based on the ^{14}C-dated tie points shown as triangles in (C) [see (*16*) for details]. Climatic events are abbreviated as follows: Hol., Holocene; YD, Younger Dryas; A-B, Allerød-Bølling; H1, Heinrich 1; and LGM, Last Glacial Maximum. (**A**) The three curves represent the C_{37} alkenone unsaturation data converted in terms of SST by using three different calibrations published by Prahl *et al.* (*40*) and Müller *et al.* (*41*) for the thick solid line with open dots [#1 in Web table 1 (*17*)], by Weaver *et al.* (*42*) for the thin solid line (#2 in Web table 1) and by Rosell-Melé *et al.* (*26*) for the thin dotted line (#3 in Web table 1). Note that the first two SST calibrations are based on the $U^{K'}_{37}$ index ($[C_{37:2}]/[C_{37:2} + C_{37:3}]$), whereas the third uses the original U^{K}_{37} index ($[C_{37:2} - C_{37:4}]/[C_{37:2} + C_{37:3} + C_{37:4}]$). As discussed in (*19*), the differences observed in some sections illustrate the overall uncertainty on the alkenone calibration. However, none of the conclusions of our study would be altered by selecting one instead of the other equation (*19*). (**B**) Black dots show the IRD in number per gram for the size fraction greater than 150 μm (Web table 1). Details about the mineralogy of the three IRD peaks are described in (*20*). The occurrences of detrital carbonates and of hematite-coated grains are specifically used to identify H events (*2*, *3*). Presence of these mineralogical markers are marked on (B) by C for detrital carbonates and H for hematite-coated grains. The IRD peak centered at 23,000 cal yr B.P. (H2a) is characterized by presence of both detrital carbonates (3%) and hematite-coated grains (2%). The small IRD peak centered at 17,500 cal yr B.P. (H1b) is mainly composed of carbonates (80%), whereas the prominent IRD peak around 16,000 cal yr B.P. (H1a) exhibits hematite-coated grains (3%) but almost no detrital carbonate. The MS record has been measured at CEREGE on discrete samples (*21*). The upper part of the core is characterized by an oxidized zone, and the MS signal is perturbed for most of the Holocene (*21*). (**C**) Percentage of $C_{37:4}$ among C_{37} alkenones, i.e., $C_{37:4}\% = 100x[C_{37:4}]/[C_{37:2} + C_{37:3} + C_{37:4}]$ with quantities based on the chromatographic peak areas.

References and Notes

1. G. C. Bond *et al.*, *Nature* **360**, 245 (1992).
2. G. Bond *et al.*, *Science* **278**, 1257(1997).
3. G. C. Bond and R. Lotti, *Science* **267**, 1005 (1995).
4. F. Grousset *et al.*, *Paleoceanography* **8**, 175 (1993).
5. J. A. Dowdeswell, M. A. Maslin, J. T. Andrews, I. N. McCave, *Geology* **23**, 301 (1995).
6. S. R. Hemming *et al.*, *Earth Planet. Sci. Lett.* **164**, 317 (1998).
7. M. Elliot *et al. Paleoceanography* **13**, 433 (1998).
8. J. A. Dowdeswell, A. Elverhoi, J. T. Andrews, D. Hebbeln, *Nature* **400**, 348 (1999).
9. H. Snoeckx, F. Grousset, M. Revel, A. Boelaert, *Mar. Geol.* **158**, 197 (1999).
10. F. Grousset, C. Pujol, L. Labeyrie, G. Auffret, A. Boelaert, *Geology* **28**, 123 (2000).
11. E. C. Grimm, G. L. Jacobson Jr., W. A. Watts, B. C. S. Hansen, K. A. Maasch, *Science* **261**, 198 (1993).
12. J. P. Sachs and S. J. Lehman, *Science* **286**, 756 (1999).
13. I. Cacho *et al.*, Paleoceanography **14**, 698 (1999).
14. C. Rühlemann, S. Mulitza, P. J. Müller, G. Wefer, R. Zahn, *Nature* **402**, 511 (1999).
15. W. F. Ruddiman, *Geol. Soc. Am. Bull.* **88**, 1813 (1977).
16. The time scale of core SU8118 used in this study is based on translating the original AMS ^{14}C ages (*17*) into calendar ages by means of the most recent ^{14}C calibrations (*35, 36*). Beyond 20,000 cal yr B.P., we also used the ^{14}C ages measured on a nearby core, MD952039, which is precisely tied to SU8118 through correlation of magnetic properties records (*21*). The ^{14}C control points used to derive the final chronology are shown as triangles on Fig. 2C. Because the total length of the core is limited to 7 m, the Late Glacial section of core SU8118 is probably free of stretching, which can occur in giant piston cores (*21*). In addition, at about 37°N latitude, the ^{14}C reservoir age probably has remained constant through time at about 400 years (*37*). By contrast, sites located farther north in the Atlantic may have experienced abrupt changes in their ^{14}C reservoir ages (*37, 38*).
17. E. Bard *et al.*, *Nature* **328**, 791 (1987).
18. Supplementary table is available at www.sciencemag.org/feature/data/1050685.shl
19. Analytical techniques used for alkenones at CEREGE are described elsewhere (*39*). The relative degree of unsaturation are expressed by the $U^{K'}_{37}$ index ($C_{37:2}/[C_{37:2} + C_{37:3}]$) or the U^{K}_{37} index ($[C_{37:2} - C_{37:4}]/[C_{37:2} + C_{37:3} + C_{37:4}]$) and the alkenone total concentration $[C_{37:2} + C_{37:3} + C_{37:4}]$ is given in μg of dry weight sediment. The precision of $U^{K'}_{37}$ measurements is about 0.01 unit (i.e., ≈ 0.3°C) and about 20% for alkenone concentrations. Figure 2A shows the temperature estimates based on a culture calibration [$T = (U^{K'}_{37} - 0.039)/0.034$; (*40*), #1 in Web table 1], which is equivalent to a global core-top compilation (*41*). In order to illustrate the effect of using different calibrations, Fig. 2A also presents two additional temperature curves: The thin curve is calculated from a regional calibration [$T = (U^{K'}_{37} - 0.186)/0.026$; (*42*), #2 in Web table 1] based on $U^{K'}_{37}$ measured in modern sediments from the northeast Atlantic (*26*). The dotted curve (#3 in Web table 1) uses the North Atlantic calibration, $T = (U^{K}_{37} - 0.093)/0.03$, based on the original definition of the U^{K}_{37} index (*26*). The maximum SST difference is <1°C during the Holocene, ~1°C during the Allerød-Bølling and the Last Glacial Maximum (LGM), but usually more than 2°C only during the last three H events. These results agree with a study of high-latitude (>65°N) sediments (*43*) suggesting that low alkenone-SSTs are more uncertain, especially when associated with IRD injections. One possible problem sometimes encountered in sediments from the northern North Atlantic is the rather low concentration of alkenones, which makes them more susceptible to contamination by reworked sediment transport. Indeed, Weaver *et al.* (*42*) measured extremely low concentrations of alkenones (<0.001 μg/g) in the glacial section of a core and suggested a contribution by older reworked alkenones. As shown in Web table 1, the C_{37} alkenone concentrations in the glacial section of core SU8118 are always rather high (>0.4 μg/g), making this problem rather unlikely. A further argument considers deep-sea currents. The modern deep circulation off Portugal is characterized by northward advection of Mediterranean outflow water (MOW) and Antarctic bottom water (AABW) bracketing the southward flow of North-Atlantic deep water (NADW) which bathes the location of SU8118. During the LGM and H events, it has been shown that the NADW flow was weaker (*44, 45*) and that the boundary between MOW and NADW was deeper (*44*). Contribution of detrital

alkenones advected by deep waters originating from high northern latitudes is thus very unlikely. A similar argument can be made against a significant contribution of NADW to the concentration of fine-grained magnetite as could occur in sediments farther north (*46*).
20. The IRD studied at DGO (Talence, France) are expressed in number per gram for the size fraction greater than 150 μm (sample size for counting is 10 g of dry sediments). The complexity of H1 and H2 is further demonstrated by their mineralogical composition: The H2a IRD peak centered at 23,000 cal yr B.P. is characterized by a dominance of quartz (84%), with a presence of feldspars (5%), detrital carbonates (3%), and hematite-coated grains (2%). Broadly similar, the H1a IRD peak at 16,000 cal yr B.P. is dominated by grains of quartz (76%) and feldspars (14%), with small percentages of hematite-coated grains (3%), glauconite (3%), volcanic shards (1%), and an almost complete lack of detrital carbonate. By contrast, the smaller IRD peak at 17,500 cal yr B.P. (H1b) is composed mainly of detrital carbonates (80%), with secondary contributions of quartz (16%) and feldspar (3%).
21. N. Thouveny *et al.*, *Earth Planet. Sci. Lett.* **180**, 61 (2000).
22. S. M. Lebreiro, J. C. Moreno, I. N. McCave, P. P. E. Weaver, *Mar. Geol.* **131**, 47 (1996).
23. M. R. Chapman and N. J. Shackleton, *Earth Planet. Sci. Lett.* **159**, 57 (1998).
24. R. Zahn *et al.*, *Paleoceanography* **12**, 696 (1997).
25. M. Zhao, N. A. S. Beveridge, N. J. Shackleton, M. Sarnthein, G. Eglinton, *Paleoceanography* **10**, 661 (1995).
26. A. Rosell-Melé, G. Eglinton, U. Pflaumann, M. Sarnthein, *Geochim Cosmochim Acta* **59**, 3099 (1995).
27. S. C. Brassell, G. Eglinton, I. T. Marlowe, U. Pflaumann, M. Sarnthein, *Nature* **320**, 129 (1986).
28. E. L. Sikes, J. K. Volkman, L. G. Robertson, J.-J. Pichon, *Geochim. Cosmochim. Acta* **61**, 1495 (1997).
29. A. Rosell-Melé, *Paleoceanography* **13**, 694 (1998).
30. H.-M. Schulz, A. Schöner, K. C. Emeis, *Geochim. Cosmochim. Acta* **64**, 469 (2000).
31. J. C. Duplessy, E. Bard, L. Labeyrie, J. Duprat, J. Moyes, *Paleoceanography* **8**, 341 (1993).
32. M. R. Chapman and M. A. Maslin, *Geology* **27**, 875 (1999).
33. R. H. Gwiazda, S. R. Hemming, W. S. Broecker, *Paleoceanography* **11**, 371 (1996).
34. T. A. Mashiotta, D. W. Lea, H. J. Spero, *Earth Planet. Sci. Lett.* **170**, 417 (1999).
35. M. Stuiver *et al.*, *Radiocarbon* **40**, 1041 (1998).
36. E. Bard, M. Arnold, B. Hamelin, N. Tisnerat-Laborde, G. Cabioch, *Radiocarbon* **40**, 1085 (1998).
37. E. Bard *et al.*, *Earth Planet. Sci. Lett.* **126**, 275 (1994).
38. T. F. Stocker and D. G. Wright, *Radiocarbon* **40**, 359 (1998).
39. C. Sonzogni *et al.*, *Deep-Sea Res. II* **44**, 1445 (1997).
40. F. G. Prahl, L. A. Muehlhausen, D. L. Zahnle, *Geochim. Cosmochim. Acta* **52**, 2303 (1988).
41. P. J. Müller, G. Kirst, G. Ruhland, I. von Storch, A. Rosell-Melé, *Geochim. Cosmochim. Acta* **62**, 1757 (1998).
42. P. P. E. Weaver *et al.*, *Paleoceanography* **14**, 336 (1999).
43. A. Rosell-Melé and P. Comes, *Paleoceanography* **14**, 770 (1999).
44. J. Schönfeld and R. Zahn, *Palaeogeogr. Palaeoclimatol. Palaeoecol.* **159**, 85 (2000).
45. L. D. Keigwin and S. J. Lehman, *Paleoceanography* **9**, 185 (1994).
46. T. M. Dokken and E. Jansen, *Nature* **401**, 458 (1999).
47. We acknowledge helpful discussions or reviews by G. C. Bond, C. De La Rocha, R. Rickaby, A. Rosell-Melé, E. L. Sikes, N. Thouveny, and anonymous referees. We thank J.-J. Motte for drawing Fig. 1. This work is supported by CNRS Programme National d'Etudes de la Dynamique et du Climat and the European Community (projects ENV4-CT97-0564, FMRX-CT96-0046, and ENV4-CT97-0659).

22 March 2000; accepted 16 June 2000

Discrete Atom Imaging of One-Dimensional Crystals Formed Within Single-Walled Carbon Nanotubes

Rüdiger R. Meyer,[1] Jeremy Sloan,[2]* Rafal E. Dunin-Borkowski,[3] Angus I. Kirkland,[1,4] Miles C. Novotny,[2] Sam R. Bailey,[2] John L. Hutchison,[3] Malcolm L. H. Green[2]

The complete crystallography of a one-dimensional crystal of potassium iodide encapsulated within a 1.6-nanometer-diameter single-walled carbon nanotube has been determined with high-resolution transmission electron microscopy. Individual atoms of potassium and iodine within the crystal were identified from a phase image that was reconstructed with a modified focal series restoration approach. The lattice spacings within the crystal are substantially different from those in bulk potassium iodide. This is attributed to the reduced coordination of the surface atoms of the crystal and the close proximity of the van der Waals surface of the confining nanotube.

The synthesis and characterization of one-dimensional (1D) crystals that have a well-specified chemistry, size, and crystal structure have presented a formidable challenge for materials chemistry and analysis. Here, we show that both the widths and the lattice spacings of 1D crystals can be tailored by encapsulating them within single-walled carbon nanotubes (SWNTs) (*1*). The resulting crystals can be tens of micrometers in length yet only two or three atoms in width. We illustrate our results for a <110> projection of a discrete KI crystal that is three atomic layers thick and formed within a SWNT, in which the crystal thickness varies in a strictly integral fashion on an atomic scale.

Conventional high-resolution transmission electron microscopy (HRTEM) has previously been used to image single heavy atoms on crystal surfaces and amorphous support films (*2–6*). The technique can be applied in the same way to provide structural information about a crystal incorporated within a SWNT. However, the image contrast is weak and noisy, and it is, in general, only possible to identify strongly scattering species such as I in an encapsulated KI crystal (see below). A single HRTEM image is also subject to artifacts due to lens aberrations such as defocus, astigmatism, and beam tilt, particularly near the edge of a crystal. These problems can be overcome by recovering the amplitude and phase of the electron wave function at the exit surface of a sample from either a focal (*7–9*) or a tilt azimuth (*10, 11*) series of images. The procedure involves the determination of the lens aberrations and a numerical reconstruction of the exit plane wave function by using a Wiener filter. The restored wave function can then be used to calculate the high-spatial-frequency components of the phase shift of the electron wave as it leaves the sample. This phase image is free of artifacts introduced by objective lens aberrations and is higher in resolution and less noisy than an individual HRTEM image. It is also less noisy than an equivalent atomic resolution phase image obtained by electron holography (*12*). For a sufficiently thin crystal, the recorded phase can be interpreted intuitively because it is directly proportional to the projected potential of the sample integrated in the incident beam direction (*13*). However, the technique imposes strict requirements on specimen and instrumental stability and must be applied with great care to SWNTs, which are damaged readily by overexposure to a high-energy electron beam.

SWNTs were synthesized with a modified high-yield arc synthesis technique (*14*) and filled with highly pure KI (99.99%) (Aldrich) through a capillary filling method (*1, 15*). The specimen was characterized at 300 kV in a Japan Electron Optics Laboratory (JEOL) JEM-3000F field emission gun transmission electron microscope (*16–18*). Figure 1A shows a phase image reconstructed from a 20-member focal series of a 1.6-nm-diameter SWNT containing a KI single crystal (*19*). In cross section, the encapsulated crystal can be regarded as a single KI unit cell viewed along

[1]Department of Materials Science, University of Cambridge, Pembroke Street, Cambridge CB2 3QZ, UK. [2]Wolfson Catalysis Centre (Carbon Nanotechnology Group), Inorganic Chemistry Laboratory, University of Oxford, South Parks Road, Oxford OX1 3QR, UK. [3]Department of Materials, University of Oxford, Parks Road, Oxford OX1 3PH, UK. [4]Department of Chemistry, University of Cambridge, Lensfield Road, Cambridge CB2 1EW, UK.

*To whom correspondence should be addressed. E-mail: jeremy.sloan@chem.ox.ac.uk